RADIO SCIENCE Journal of Research NBS/USNC–URSI
Vol. 69D, No. 6, June 1965

The Biexponential Nature of Tropospheric Gaseous Absorption of Radio Waves[1]

E. J. Dutton and B. R. Bean

Central Radio Propagation Laboratory, National Bureau of Standards, Boulder, Colo.

(Received January 28, 1965; revised February 1, 1965)

This paper discusses the characteristics, and some of the statistics of the general climatological aspects of considering atmospheric oxygen and water vapor absorption (the two principal contributors to atmospheric gaseous absorption in the 6 to 45 Gc/s frequency range) to be decreasing exponential functions of height from their surface value. The paper is intended primarily as an examination of these climatological aspects and the maps included are not primarily intended for application. The dry (oxygen) term of this biexponential model is extremely well behaved, but the wet (water vapor) term depends on time of year, geographic location, air mass, and general climatology of the areas for which application is intended.

Gaseous absorption of radio energy in the 6 to 45 Gc/s frequency range arises principally from water vapor and oxygen. The combined absorption may be represented by a biexponential decrease from the surface values. The oxygen absorption is well described by the model, as is water vapor absorption except in regions of very low water vapor content.

1. Introduction

In the frequency range 6 to 45 Gc/s, the atmospheric, gaseous absorption, γ, at a particular frequency, expressed in dB/km, arises primarily from oxygen (dry) absorption, γ_d, and water vapor (wet) absorption, γ_w; i.e.,

$$\gamma=\gamma_d+\gamma_w. \tag{1}$$

Zhevankin and Troitskii [1959] have indicated that γ_d and γ_w can be represented as exponential functions of height, z, above the earth's surface,

$$\gamma_d=\gamma_{d,0}\exp\left(\frac{-z}{H_d}\right),\ \gamma_w=\gamma_{w,0}\exp\left(\frac{-z}{H_w}\right), \tag{2}$$

where $\gamma_{d,0}$ and $\gamma_{w,0}$ are the values of γ_d and γ_w, respectively, at the earth's surface, and H_d and H_w are called the "scale heights" of γ_d and γ_w. This model is known as the "biexponential" model of absorption. The values of γ_d and γ_w are often called the "dry" and "wet" terms of γ.

This paper primarily examines the possible extent to which this model can be employed on a worldwide climatological basis, to either support or not support application of the model at a given location. Since the data used in this paper are not extensive, the paper is not primarily intended to be used in applications. More extensive data taken during the seasons discussed are advisable to meet this end.

The scale height for the dry term in the 6 to 45 Gc/s frequency range can be written as

$$H_d=\frac{T_0}{c+b\alpha}, \tag{3}$$

where T_0 is the surface absolute temperature, α is the temperature lapse rate with height, which is assumed to be a constant for the entire atmosphere, and b and c are constants determined from thermodynamic considerations.

2. Statistical Fitting of the Biexponential Model

Radiosonde data for 49 climatically and geographically diverse stations were fit, by means of a least squares regression method, to the biexponential absorption model. Two radiosonde profiles for each station were chosen, one in the month of February, the other in the month of August. Each profile was so chosen as to be *reasonably representative* of average wintertime and summertime meteorological conditions at the site where the profile was obtained.

[1] This paper was presented at the World Conference on Radio Meteorology, Sept. 14–18, 1964, National Bureau of Standards, Boulder, Colo.

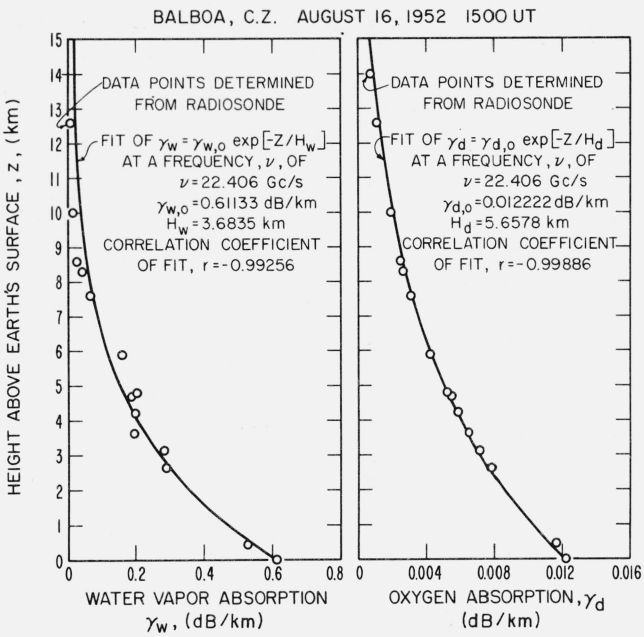

FIGURE 1. *Exponential fits to oxygen and water vapor absorption versus height at Balboa, Canal Zone.*

TABLE 1. *Fit of* $\gamma_d = \gamma_{d,0} \exp[-z/H_d]$

Frequency	Surface oxygen absorption	Scale height	Correlation coefficient of fit	Standard error of estimate of γ_d, S. E.
ν	$\gamma_{d,0}$	H_d	r	
	at Barrow, Alaska, February 20, 1952, 0500 UT			
Gc/s	*dB/km*	*km*		*dB/km*
6.0	0.01167	3.5616	−0.99473	±0.00032
22.406	.02374	3.5387	−.99463	±.00067
42.0	.17433	3.5568	−.99471	±.00486
	at Sopporo, Japan, August 26, 1952, 1500 UT			
6.0	0.00651	5.1677	−0.99980	±0.00004
22.406	.01322	5.1449	−.99979	±.00008
42.0	.09724	5.1630	−.99980	±.00060
	at Balboa, Canal Zone, August 16, 1952, 1500 UT			
6.0	0.00602	5.6825	−0.99883	±0.00009
22.406	.01222	5.6578	−.99887	±.00018
42.0	.08994	5.6773	−.99883	±.00137
	at Denver, Colo., U.S.A., August 16, 1952, 0300 UT			
6.0	0.00447	5.5955	−0.99915	±0.00006
22.406	.00906	5.5789	−.99917	±.00012
42.0	.06680	5.5920	−.99915	±.00090
	at Guryev, U.S.S.R., August 23, 1957, 0000 UT			
6.0	0.00685	5.0330	−0.99161	±0.00024
22.406	.01391	5.0102	−.99152	±.00049
42.0	.10229	5.0283	−.99159	±.00362

TABLE 2. *Fit of* $\gamma_w = \gamma_{w,0} \exp[-z/H_w]$

Frequency	Surface water vapor absorption	Scale height	Correlation coefficient of fit	Standard error of estimate of γ_w, S. E.
ν	$\gamma_{w,0}$	H_w	r	
	at Barrow, Alaska, February 20, 1952, 0500 UT			
Gc/s	*dB/km*	*km*		*dB/km*
6.0	0.00006	−2.7747	+0.64063	±0.00277
22.406	.00498	−2.3254	+.73546	±.62074
42.0	.00245	−2.7792	+.63995	±.11748
	at Sopporo, Japan, August 26, 1952, 1500 UT			
6.0	0.00418	2.4989	−0.97903	±0.00018
22.406	.48160	4.1971	−.95934	±.03513
42.0	.17860	2.4961	−.97912	±.00777
	at Balboa, Canal Zone, August 16, 1952, 1500 UT			
6.0	0.00513	2.1796	−0.99832	±0.00007
22.406	.61133	3.6835	−.99256	±.02475
42.0	.21928	2.1772	−.99833	±.00300
	at Denver, Colo., U.S.A., August 16, 1952, 0300 UT			
6.0	0.00198	1.8196	−0.98591	±0.00007
22.406	.32502	2.4972	−.96403	±.01779
42.0	.08476	1.8185	−.98595	±.00279
	at Guryev, U.S.S.R., August 23, 1957, 0000 UT			
6.0	0.00262	2.5987	−0.74450	±0.00033
22.406	.29374	4.1792	−.65330	±.04856
42.0	.11190	2.5952	−.74489	±.01420

Figure 1 shows an example of one of these profiles for Balboa, Canal Zone, on a typical August day. On figure 1 are plotted the data points of both water vapor and oxygen absorption determined from the meteorological parameters obtained during the radiosonde ascent. Also plotted on figure 1 are the exponential fits [as in (2)] resulting from least squares regression of the data in the figure. Tables 1 and 2 also show some of the data for exponential fits of oxygen and water vapor absorption.[2] Note that Barrow, Alaska, in table 2, a poor fit for the water vapor absorption, has *negative* H_w's and positive correlation coefficients. This implies that γ_w in this case is actually better represented by an increasing exponential function of height rather than by a decreasing exponential function, and points out a phenomenon peculiar to arctic wintertime conditions.

Figures 2 and 3 show H_d and H_w as functions of frequency at a near arctic (Verkhoyansk, U.S.S.R.) location and at a tropical (Balboa, Canal Zone) location. The spectra of H_d and H_w for the two stations plotted in figures 2 and 3 were obtained from two least squares regression fits. Each of the two regression fits were from radiosonde data composing a given single profile which was used as *representative* of seasonal condi-

[2] A forthcoming NBS Technical Note on the material covered in this paper will include the complete data of the 49 station sample analogous to tables 1 and 2. These tables will include regressions for many more frequencies in the 6–45 Gc/s range.

tions at the station. Each plot shows the variation of H_d and H_w in the location from summer (August) to winter (February). It is important to note the constancy with respect to frequency of the H_d curves even at the water vapor resonance frequency, 22.4 Gc/s. Thus, a single value of H_d determined from (3) may be used to represent H_d in the 6–45 Gc/s range, but a different value of H_w is required for each frequency.

Figures 4, 5, 6, and 7 are plots of H_d versus $\gamma_{d,0}$ and H_w versus $\gamma_{w,0}$ using as data the results of the least squares biexponential fits discussed above on the 49 stations. These figures also include the wintertime (February) and the summertime (August) values on the same chart. Figure 4 shows H_d versus $\gamma_{d,0}$ at a wavelength, λ, of 3 cm—well off water vapor resonance, and figure 5 shows H_d versus $\lambda_{d,0}$ at water vapor resonance, $\lambda \cong 1.33$ cm.

A least squares fit to the data of figures 4 and 5 of the form:

$$H_d = B\gamma_{d,0} + A, (A \text{ and } B \text{ are constants}) \qquad (4)$$

gives reasonably high correlation coefficients, r, of -0.78 and -0.76 as seen on the figures. This is understandable, on the basis of (3), which strongly indicates the dependence of H_d on surface conditions.

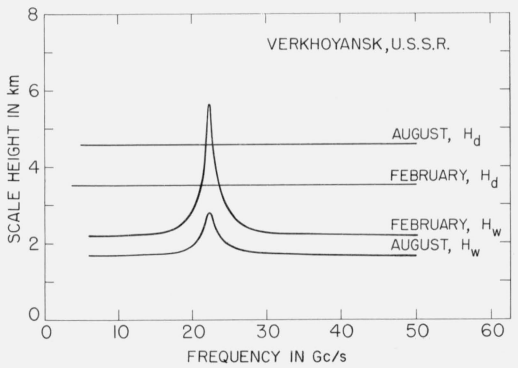

FIGURE 2. *Dry and wet term scale heights versus frequency at Verkhoyansk, U.S.S.R.*

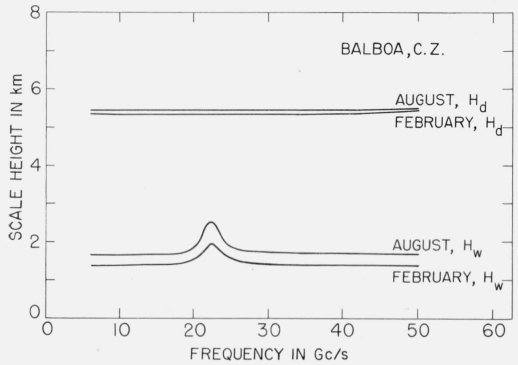

FIGURE 3. *Dry and wet term scale heights versus frequency at Balboa, Canal Zone.*

However, the data do not support the strong possibility of the similar expression,

$$H_w = C\gamma_{w,0} + D, (C \text{ and } D \text{ are constants}) \qquad (5)$$

for water vapor, as seen on figures 6 and 7.

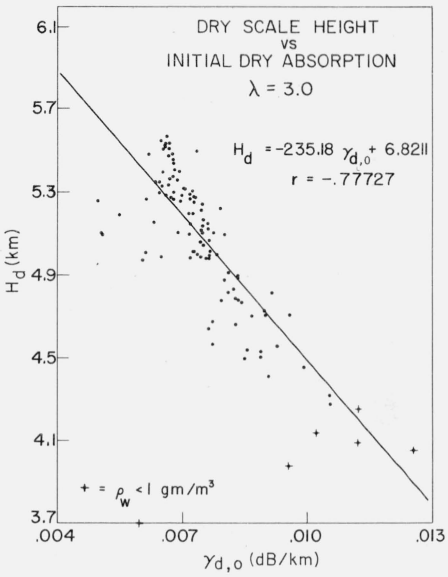

FIGURE 4. H_d *versus* $\gamma_{d,0}$ *away from the* $\gamma = 1.33$ *cm water vapor resonance.*

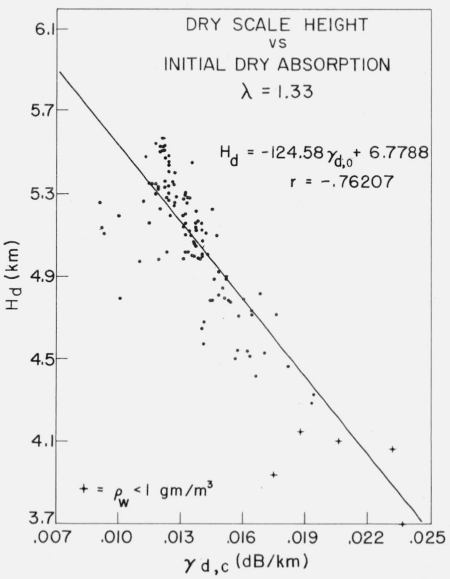

FIGURE 5. H_d *versus* $\gamma_{d,0}$ *near the* $\gamma = 1.33$ *cm water vapor resonance.*

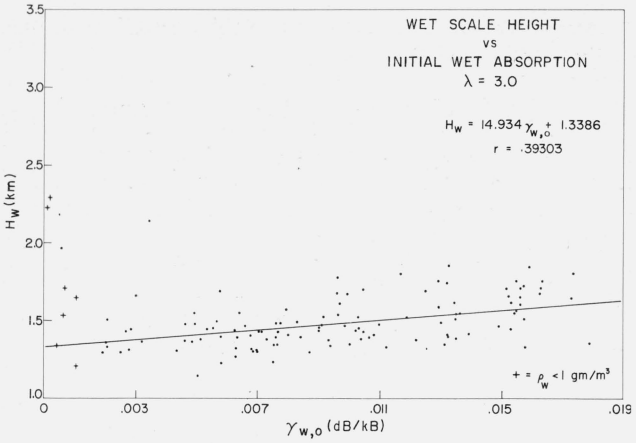

FIGURE 6. H_w *versus* $\gamma_{w,0}$ *away from the* $\gamma = 1.33$ *cm water vapor resonance.*

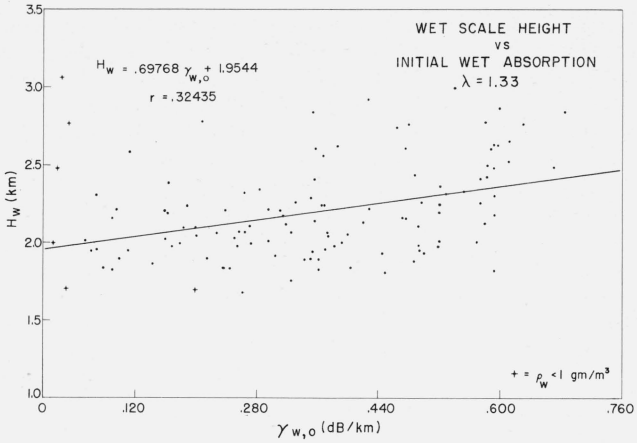

FIGURE 7. H_w *versus* $\gamma_{w,0}$ *near the* $\gamma = 1.33$ *cm water vapor resonance.*

TABLE 3. *Values of actual total integrated absorption,* $\tau_a = \int_0^\infty \gamma ds$, *and exponentially computed values* $\tau_{exp} = \tau_d + \tau_w$ *where* $\tau_d = \int_0^\infty \gamma_{d,o}$ $exp\left(\frac{-z}{H_d}\right) dz$, $\tau_w = \int_0^\infty \gamma_{w,o}\, exp\left(\frac{-z}{H_w}\right) dz$, $\theta_0 = 90°$

Frequency	Balboa, Canal Zone (August)					Sopporo, Japan (August)					Barrow, Alaska (February)				
	τ_a	τ_{exp}	τ_0	τ_w	$\delta\tau = \tau_a - \tau_{exp}$	τ_a	τ_{exp}	τ_d	τ_w	$\delta\tau$	τ_a	τ_{exp}	τ_d	τ_w	$\delta\tau$
Gc/s	*dB*	*dB*	*dB*	*dB*	*dB*										
6.0	0.043	0.045	0.034	0.011	−0.002	0.042	0.044	0.034	0.010	−0.002	0.043	0.042	0.042	0	+0.001
22.406	2.119	2.321	.069	2.252	−.202	1.945	2.089	.068	2.021	−.144	0.143	.072	0.084	−0.012	+.071
42.0	0.949	0.988	.511	0.477	−.039	0.911	0.948	.502	0.446	−.037	0.655	.613	0.620	−.007	+.042

Table 3 shows a comparison of total integrated absorption, $\int_0^\infty \gamma ds$, through the entire atmosphere calculated from actual radiosonde data and the total integrated absorption obtained from fits of the bi-exponential model (s is the path length). There are three stations chosen, Balboa, Canal Zone (August), representing tropical conditions, Sopporo, Japan (August), representing temperate conditions, and Barrow, Alaska (February), representing arctic conditions. Each station is examined at three different frequencies: 6 Gc/s and 42 Gc/s on both sides of water vapor resonance, and the water vapor resonance frequency, 22.406 Gc/s. The initial elevation angle, θ_0, of the path is taken to be 90°, for purposes of simple integration of the exponential model. It is worthwhile to note that, even for the worst fits (wet exponential fit of Barrow, Alaska, which, as mentioned before, fit best with a negative H_w, thus accounting for the negative values of τ_w) the error in the total integrated absorption is not any larger than the other errors listed in table 3.

3. Climatology of Surface Dry and Wet Absorptions

A discussion of the equations for absorption in the 6 to 45 Gc/s frequency range, and how these equations depend upon the commonly measured meteorological parameters of pressure, P, temperature, T, and water vapor density, ρ_w, can be found in Bean [1964]. It is these formulas that were used for absorption computations on the profiles for the 49 stations mentioned earlier. The surface values of absorption from this 49 station sample, were used as the basis for the contours drawn in figures 8, 9, 10, and 11. Figure 8 shows contours of $\gamma_{d,0}$ for a wavelength of 3 cm under wintertime (February) conditions, and figure 9 shows $\gamma_{d,0}$ contours for a 3 cm wavelength in the summertime (August). Regardless of their numerical value, for a particular contour map $\gamma_{d,0}$ and $\gamma_{w,0}$ should behave essentially the same at all frequencies in the range 6 to 45 Gc/s, at least as far as meteorological and/or latitudinal variation is concerned. In figure 8, for example, a decided seasonal effect is noticed immediately for this wintertime case when compared with the summertime picture of figure 9. The seasonal effect

is the fact that near the equator the values of $\gamma_{d,0}$ remain essentially unchanged from summer to winter, but much higher values of $\gamma_{d,0}$ are evident in arctic and upper northern hemisphere locations in the winter than in the summer, and vice versa for the antarctic and lower southern hemisphere locations.

This variation is understandable if one recalls that $\gamma_{d,0}$ is directly proportional to pressure, p_0, at the surface [Van Vleck, 1951]. Worldwide maps of average seasonal surface pressures show a decided analogy to figures 8 and 9 as regards the appearance of the contours.

Figures 10 and 11 show maps of $\gamma_{w,0}$ for wintertime (February) and summertime (August) conditions, where the values of $\gamma_{w,0}$ were obtained from the 49 station sample discussed earlier. Because of the direct proportionality of $\gamma_{w,o}$ to surface water vapor density, $\rho_{w,0}$ [Van Vleck, 1951], the most noticeable trend on figure 10 is the contenental-to-ocean change in $\gamma_{w,0}$ especially in the northern hemisphere. This trend, no doubt, reflects the contrast of maritime air and the cold, dry air masses common to the interior of continents at this time of year. Surprisingly, at first, there seems not to be nearly so much of a similar effect in figure 11 in the antarctic region, but this is undoubtedly because there is so much more ocean between southern hemisphere continents than in the northern hemisphere.

Figures 12 and 13 show the worldwide character of the dry absorption scale height, H_d, as determined from the 49 station sample. Again because of the independence of (3) with wavelength, climatic variations on either map at one particular wavelength is representative of climatic variations for all wavelengths in the 6 to 45 Gc/s frequency range. Figure 12 represents wintertime H_d (February) conditions for a wavelength of $\lambda = 1.339$ cm, and figure 13 represents summertime H_d (August) conditions at a wavelength of $\lambda = 3.0$ cm. Note in general the latitudinal trend of the scale heights which closely follows the seasonal surface temperature trends for the world, again as expected from (3).

Figures 14 and 15 represent the worldwide trend of the wet absorption scale height, H_w, as determined from the 49 station sample. However, figures 2 and 3 show that the essential important difference between H_d and H_w in the 6 to 45 Gc/s frequency range is the maximum in the H_w curve near water vapor resonance (22.4 Gc/s). This, of course, shows that H_w is not independent of frequency. However, it can be shown that between 6 and 45 Gc/s:

$$\frac{1}{H_w} \cong f_1(\rho_w) + f_2(P, T_0) + f_3(\lambda, T_0) \tag{6}$$

where $f_1(\rho_w)$ is a function of water vapor density, ρ_w, alone, and for that matter

$$f_1(\rho_w) \equiv \frac{1}{H_{\rho_w}} \tag{7}$$

where H_{ρ_w} is the scale height of an assumed exponential fit of the form

$$\rho_w = \rho_{o,\,w} \exp -\left(\frac{z}{H_{\rho_w}}\right) \tag{8}$$

to the water vapor density profile where $\rho_{0,w}$ is the surface value of ρ_w. The function $f_2(P, T_0)$ in (6) is a function of atmospheric pressure P, and surface temperature T_0, and $f_3(\lambda, T_0)$ is a function of wavelength and surface temperature.

By differentiating (6), we obtain

$$-\frac{1}{H_w^2}\Delta H_w = \Delta f_1 + \Delta f_2 + \Delta f_3. \tag{9}$$

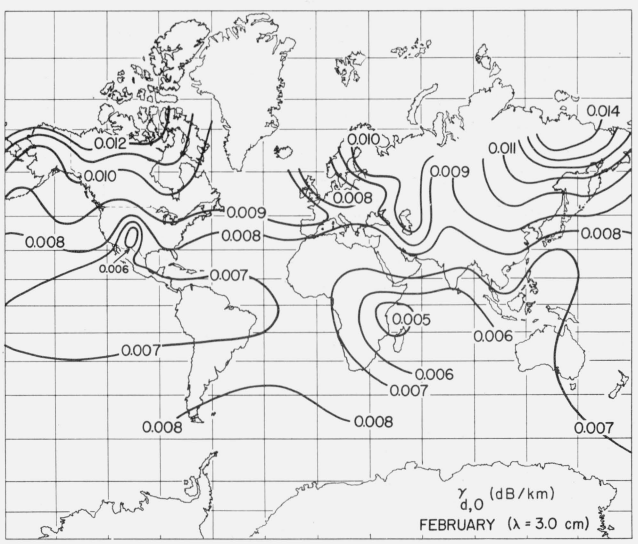

FIGURE 8. *Characteristic worldwide wintertime (February) values of* $\gamma_{d,0}$.

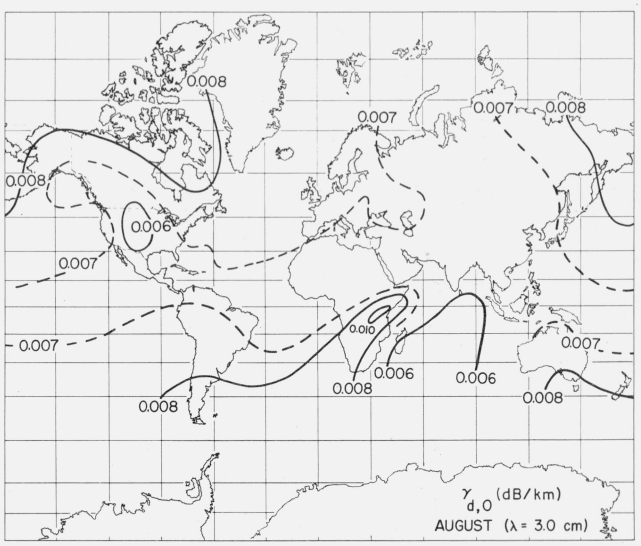

FIGURE 9. *Characteristic worldwide summertime (August) values of* $\gamma_{d,0}$.

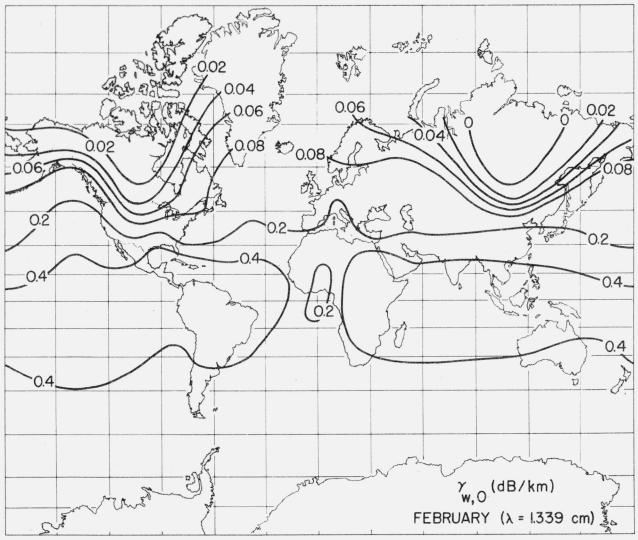

FIGURE 10. *Characteristic worldwide wintertime (February) values of* $\gamma_{w,0}$.

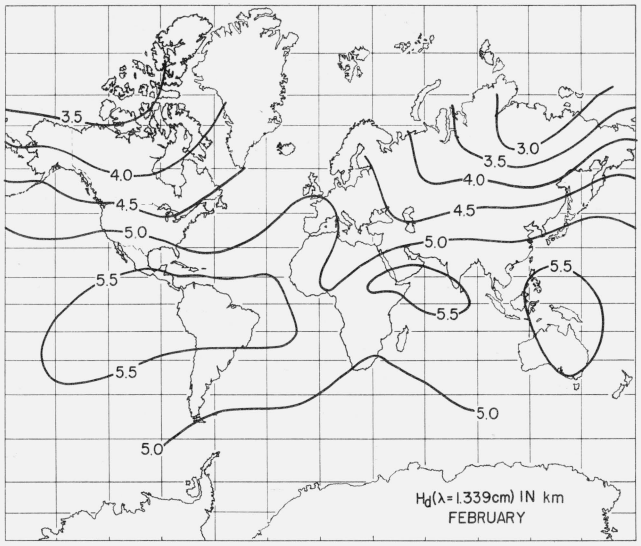

FIGURE 12. *Characteristic worldwide wintertime (February) values of* H_d.

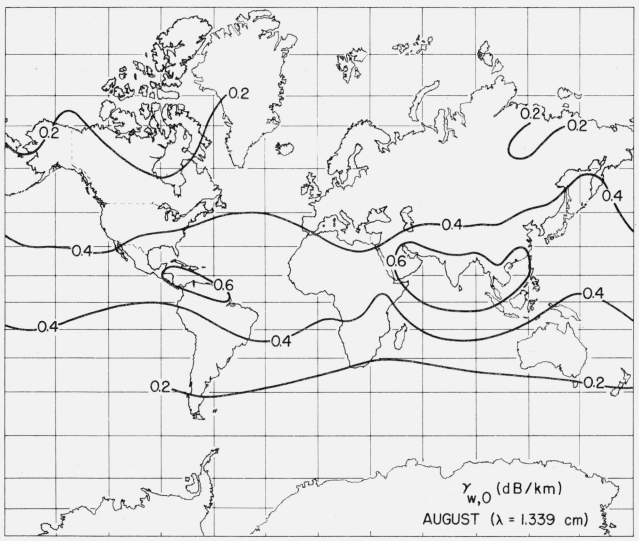

FIGURE 11. *Characteristic worldwide summertime (August) values of* $\gamma_{w,0}$.

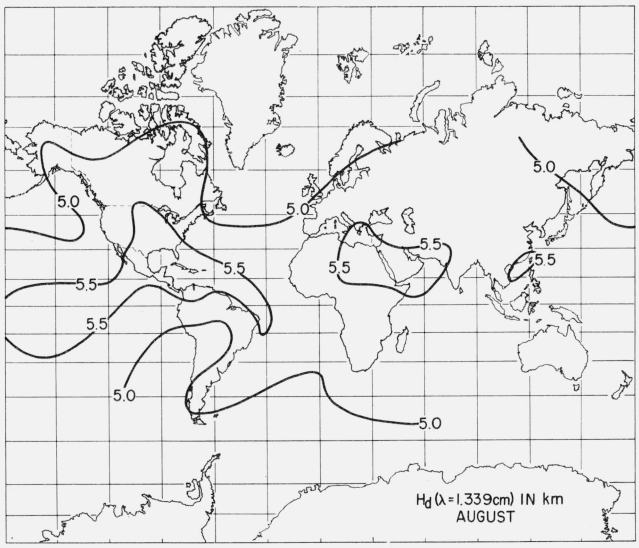

FIGURE 13. *Characteristic worldwide summertime (August) values of* H_d.

The Δf_3 term of (9) is unchanged, if temperature is unchanged, from location to location in figures 14 and 15. Similarly, it would be unchanged on any other H_w map from location to location when that map is plotted for a given frequency. For the normal atmospheric range of temperature conditions, Δf_3 generally contributes less than 10 percent of (9). For the given conditions of figures 14 and 15, the *variations* of H_w on any other map plotted for a *different* frequency should remain about the same. Hence the seasonal climatic variations of H_w for the frequency spectrum 6 to 45 Gc/s are characterized in figures 14 and 15. It is interesting to note that for $H_{\rho_w} \leq 2.5$ km, where H_{ρ_w} values are frequently clustered, f_1 constitutes 85 percent or more of the total contribution to (6).

Figure 14 indicates the wintertime (February) variation of H_w (at $\lambda = 1.339$ cm), and figure 15 indicates the summertime (August) variation of H_w (at $\lambda = 1.339$ cm). The most important climatic feature to be noted on both maps is the continental-oceanic effect, but there are also effects depending upon the actual climatic character of a particular area. For example, in the summer there is a drop (fig. 15) in H_w values towards the interior of North America. This is probably caused by the general continental tropical (dry) conditions that tend to prevail over the continent in the summer. The cross-hatched area in figure 14 represents regions of very poor fit of the biexponential model. These are the arctic cases, as indicated in table 4. Their presence is more severely felt

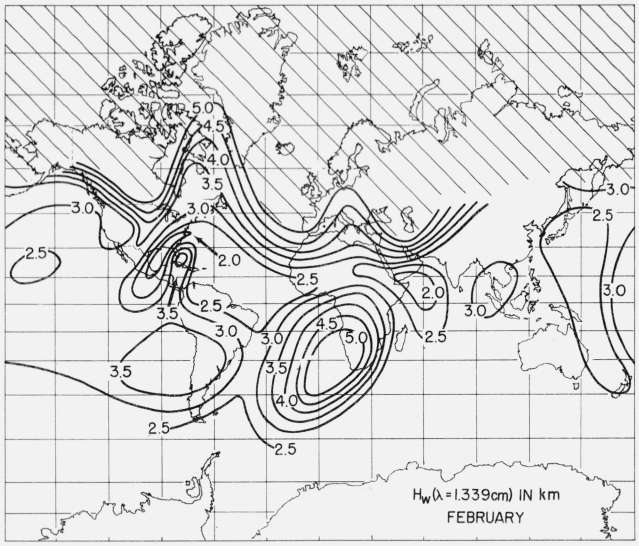

FIGURE 14. *Characteristic worldwide wintertime (February) values of* H_w.

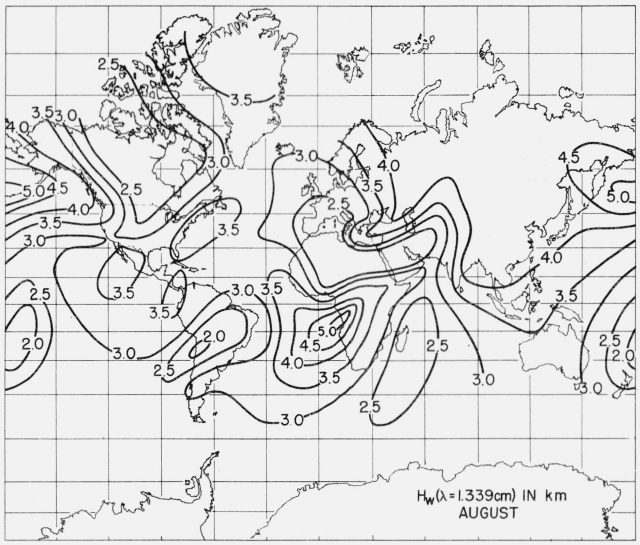

FIGURE 15. *Characteristic worldwide summertime (August) values of* H_w.

in the northern hemisphere in the winter (fig. 14) than in the summer (fig. 15) where, except at the poles, no appreciable arctic effect is present.

TABLE 4. *Average correlation coefficients,* $\bar{r}$, *and standard errors of estimate* $\overline{S.E.}$ *of a fit of the form of* $\gamma_w=\gamma_{w0}\exp(-z/H_w)$ *at* $\lambda=1.339$ *cm to radiosonde data of several stations geographically widely dispersed.*

Air mass	Number of pieces of data averaged	Mean surface temperature $\overline{T_0}$	Mean surface relative humidity $\overline{RH_0}$	$\bar{r}$	$\overline{S.E.}$
		°C	%		*dB/km*
cA($T>-30$ °C)	7	−15.9	80	−0.0065	±0.01796
mT	55	+21.8	79	−0.9191	±0.03997
Combined cases: cP + mP + cT	24	+6.1	76	−0.9098	±0.01942

4. Climatology of Individual Biexponential Fits

Since the oxygen absorption is easily fit with a descending exponential function of height with a correlation coefficient of −0.99 or better for all the cases tested in the 49-station sample, the most concern from location to location is the water vapor or wet absorption. One can easily find two different stations, even with quite similar geography and with quite similar surface meteorological conditions, yet exponential fits to their radiosonde profiles yield two very different values of scale heights, H_w, correlation coefficients, r, and standard errors of estimate, S.E. Likewise, the same station under different synoptic weather conditions can have widely differing exponential fits. Unfortunately, unlike in the biexponential model of the refractive index [Bean, 1961] in the 6 to 45 Gc/s region, the wet term of absorption usually tends to dominate the total integrated absorption (see figs. 8–11 for typical values), especially near water vapor resonance, $\lambda=1.339$ cm, thus making it relatively imperative that the wet term exponential fit be closely examined climatologically.

Perhaps the easiest climatological approach is classification of air masses according to source in standard meteorological fashion [Byers, 1944; Willett, 1944] as:

(a) Continental Arctic (cA)
(b) Maritime Tropical (mT)
(c) Maritime Polar (mP)
(d) Continental Polar (cP)
(e) Continental Tropical (cT).

It would, of course, be necessary to examine the records of any particular location fully and perhaps, if frontal transitions are common, to consider mixed air masses [combinations of (a) through (e)] in order to determine the goodness of an exponential fit to the wet absorption. However, based on a study of 86 worldwide cases, table 4 helps to shed some light on the problem.

The air masses were chosen from Willett's [1944] classification for the time of year considered. In table 4, one observes that the average correlation coefficient for cA cases is quite low. This is a uniform tendency caused largely by the surface temperature inversions noted in such air masses, and probably to some degree by the fact that radiosondes' humidity elements perform poorly at temperatures below 0 °C [Wexler, 1949]. If the latter condition were corrected, the correlation coefficients in cA air masses might be considerably higher. It is also important to note that although the correlation coefficient is so low, the average standard error of estimate, S.E., is not very large. However, table 4 also shows that in spite of the much higher average correlation coefficient, an exponential model applied to the wet term for mT air mass cases might cause serious difficulties depending upon the application at hand.

5. Conclusions

It has been seen that the fit of a biexponential model to atmospheric absorption with height is exceptionally good for the dry term from 6 to 45 Gc/s and is generally good for the wet term in this frequency range except in cA cases where the wet term is small. An individual application requires the caution of the user and he should study his particular area climatologically and synoptically, depending upon the extent to which he plans application of the biexponential model.

The authors wish to acknowledge the helpful advice, computer programs, and criticism of C. A. Samson, R. L. Abbott, E. R. Westwater, W. B. Sweezy, M. T. Decker, K. A. Norton, and R. E. McGavin in the preparation of this paper.

6. References

Bean, B. R. (1961), Concerning the biexponential nature of the tropospheric radio refractive index, Beiträge zur Physik der Atmosphäre, Bd. **34,** Heft 1/2, 81–91.

Bean, B. R. (1964), Attenuation of radio waves, ch. from Advances in Radio Research, 121–156 (Academic Press Inc., London).

Byers, H. R. (1944), General Meteorology, 255–292 (McGraw-Hill Book Co. Inc., New York, N.Y.).

Van Vleck, J. H. (1951), Theory of absorption of uncondensed gases, Propagation of Short Radio Waves, D. E. Kerr, ed., 646–664. (McGraw-Hill Book Co. Inc., New York, N.Y.).

Wexler, A. (July 1949), Low temperature performance of radiosonde electric hydrometer elements, J. Res. NBS **43,** 49–56.

Willett, H. C. (1944), Descriptive Meteorolgy, 183–224, (Academic Press, Inc., New York, N.Y.).

Zhevankin, S. A., and V. S. Troitskii (1959), Absorption of centimeter waves in the atmosphere, Radio Technika i Elektronika **4,** No. 1, 31–41.

(Paper 69D6–522)